The secreted neurotrophin Spätzle 3 promotes glial morphogenesis and supports neuronal survival and function

Jaeda C. Coutinho-Budd,[1] Amy E. Sheehan,[2] and Marc R. Freeman[2]

[1]Department of Neurobiology, University of Massachusetts Medical School, Worcester, Massachusetts 01605, USA; [2]Vollum Institute, Oregon Health and Sciences University, Portland, Oregon 97239, USA

Most glial functions depend on establishing intimate morphological relationships with neurons. Significant progress has been made in understanding neuron–glia signaling at synaptic and axonal contacts, but how glia support neuronal cell bodies is unclear. Here we explored the growth and functions of *Drosophila* cortex glia (which associate almost exclusively with neuronal cell bodies) to understand glia–soma interactions. We show that cortex glia tile with one another and with astrocytes to establish unique central nervous system (CNS) spatial domains that actively restrict glial growth, and selective ablation of cortex glia causes animal lethality. In an RNAi-based screen, we identified αSNAP (soluble NSF [N-ethylmalemeide-sensitive factor] attachment protein α) and several components of vesicle fusion and recycling machinery as essential for the maintenance of cortex glial morphology and continued contact with neurons. Interestingly, loss of the secreted neurotrophin Spätzle 3 (Spz3) phenocopied αSNAP phenotypes, which included loss of glial ensheathment of neuron cell bodies, increased neuronal cell death, and defects in animal behavior. Rescue experiments suggest that Spz3 can exert these effects only over very short distances. This work identifies essential roles for glial ensheathment of neuronal cell bodies in CNS homeostasis as well as Spz3 as a novel signaling factor required for maintenance of cortex glial morphology and neuron–glia contact.

[*Keywords*: glia; neurotrophin; *Drosophila*; cortex glia; spz3; αSNAP]

Supplemental material is available for this article.

Received August 8, 2017; revised version accepted October 20, 2017.

The major glial subtypes in the mammalian central nervous system (CNS)—astrocytes, microglia, oligodendrocytes, and oligodendrocyte precursor cells (OPCs)—are quite distinct morphologically and were initially parsed into these glial subclasses based on their different cellular architectures. Their unique architectures likely evolved to optimize neuron–glia signaling in the context of their specific physiological functions. Major areas of focus in recent studies of glial biology include roles for astrocytes in synapse formation and pruning (Christopherson et al. 2005; Chung et al. 2013; Tasdemir-Yilmaz and Freeman 2014) and circuit function (Paukert et al. 2014; Ma et al. 2016), the role of microglia as the brain's immune cells that survey the parenchyma and remove neuronal debris (Nimmerjahn et al. 2005), and oligodendrocyte ensheathment and support of axons (Sherman and Brophy 2005). However, all major CNS glial subtypes also include cells that interact closely with neuronal cell bodies. Protoplasmic astrocytes form extensive contacts on neuronal cell bodies (Allen and Barres 2009), satellite microglia form contacts between their cell bodies and those of neurons (Baalman et al. 2015), and even specialized groups of perineuronal oligodendrocytes have been shown to reside on neuronal cell bodies (Takasaki et al. 2010; Battefeld et al. 2016). Glial association with neuronal cell bodies is particularly extensive in mammalian peripheral ganglia, where satellite glial cells surround and isolate individual neuronal cell bodies (Christie et al. 2015). While soma-associated satellite glia have emerged as important modulators of pain after peripheral nerve injury (Huang et al. 2013), we understand very little about signaling events between any type of glial process and the cell bodies of neurons.

The insect CNS is compartmentalized into two primary regions: the cell cortex (consisting of neuronal cell bodies and their proximal axons) and the synaptic neuropil (containing all CNS neurites and synapses) (Supplemental Fig. S1). Specialized glial subtypes are also compartmentalized into these brain regions. For example, astrocyte

Corresponding authors: freemmar@ohsu.edu, jaeda.coutinho-budd@umassmed.edu

Article published online ahead of print. Article and publication date are online at http://www.genesdev.org/cgi/doi/10.1101/gad.305888.117.

processes in the *Drosophila* CNS are confined to the neuropil, which is devoid of neuronal cell bodies, and these astrocytes associate primarily with synapses, axons, and dendrites (Stork et al. 2014). *Drosophila* astrocytes are well conserved with mammalian protoplasmic astrocytes in terms of their ramified morphology, tiling behavior, expression profiles, and functions in synapse formation (Muthukumar et al. 2014; Stork et al. 2014), synaptic pruning (Tasdemir-Yilmaz and Freeman 2014), and regulation of synaptic function (Ma et al. 2016). Cortex glia, in contrast, are restricted to the cell cortex region, which is devoid of synapses (Pereanu et al. 2005; Awasaki et al. 2008). Cortex glia extend fine processes that infiltrate the entire cell cortex region with a lattice-like structure: Their processes span from the surface of the cortex to the edge of the synaptic neuropil, encapsulating virtually every neuronal cell body in the CNS (Awasaki et al. 2008). Based on analysis in the adult lamina and central brain, it is estimated that a single cortex glial cell may encase up to 100 neurons in the adult (Kremer et al. 2017). Given these tight cellular associations, cortex glia are thought to provide metabolic support and key nutrients to neurons (Volkenhoff et al. 2015) and have been shown to exhibit local Ca^{2+} transients close to neuronal cell bodies that may be essential for neuronal function (Melom and Littleton 2013).

Incisive studies of glial interactions with neuronal cell bodies have been hindered by a lack of tools with which to directly assay glial function at neuronal cell bodies in the intact nervous system. Here we developed new tools that allow for precise labeling and genetic manipulation of cortex glia throughout *Drosophila* development, from the level of single cells to the entire population. Using these tools, we show that cortex glia rapidly infiltrate the cortex region of the ventral nerve cord (VNC) at late embryogenesis and tile with themselves and astrocytes to establish unique spatial domains around neuronal cell bodies. Surprisingly, we found that cortex glia and astrocytes reciprocally inhibit each other's growth to actively demarcate the CNS cortex–neuropil boundary. We performed a large-scale RNAi-based screen for genes required in cortex glial morphogenesis and identified multiple components of vesicle fusion and recycling machinery as well as the secreted neurotrophin Spätzle 3 (Spz3) as required for maintenance of cortex glia–neuron interactions. Loss of association between cortex glia and neuronal cell bodies resulted in neuronal cell death and behavioral impairment, arguing that active maintenance of cortex glial morphology and signaling to neuronal cell bodies is essential for proper nervous system function.

Results

Cortex glia rapidly extend processes between neuronal cell bodies to establish nonoverlapping spatial domains

Mature cortex glia ensheath nearly every neuronal cell body individually in the larval and adult *Drosophila* CNS. Their processes are thought to span the entire cortex region, extending from the subperineurial glia (SPGs)—which, together with perineurial glia, make up the blood–brain barrier surrounding the CNS—to the ensheathing glia and astrocytes at the synaptic neuropil (Supplemental Fig. S1). We sought to define the developmental events that lead to the establishment of these morphological relationships and generate tools with which to explore the cellular and molecular basis of cortex glial interactions with other CNS cell types.

A number of *Gal4* drivers have been reported to express in cortex glia in *Drosophila* larval and adult brains; however, we found that all of these drivers are expressed at significant levels in additional cell types (e.g., neuropil glia, surface glia, or neurons) (Supplemental Fig. S2). To identify a *Gal4* driver line that was selective for expression in cortex glia, we screened CNS expression pattern images from a collection of ~7000 enhancer–Gal4 driver lines (Pfeiffer et al. 2008; Jenett et al. 2012). We selected several candidates with potential expression in cortex glia and assessed top candidates in more detail. One of these lines, *GMR54H02-Gal4*, which uses the 932-base-pair (bp) sequence of the first intron of *wrapper* to drive Gal4 expression, was largely specific to cortex glia, although we noted expression in surface glia and additional non-nervous system tissue such as Malpighian tubules (Supplemental Fig. S3). We further generated cortex glial driver lines for other binary expression systems (*wrapper932i-LexA* and *wrapper932i-QF2*) as well as *wrapper932i-gal80* for the purposes of repressing Gal4 expression selectively in cortex glia. When we crossed *wrapper932i-Gal80* into all previously characterized cortex glial Gal4 driver backgrounds, we confirmed that all lines had significant expression in many additional glial or neuronal subtypes (Supplemental Fig. S2). To generate a precise cortex glia-specific driver line, we used split Gal4 intersectional expression technology (Luan et al. 2006). Briefly, we used the *GMR54H02-Gal4* enhancer to drive expression of the DNA-binding domain (DBD) of Gal4 in conjunction with a 3.5-kb *Nrv2* promoter that is specific to nonsurface glial subtypes to drive expression of the VP16 transcription activation domain (*wrapper932i-Gal4DBD,Nrv2-VP16AD*, referred to here as *CtxGlia-SplitGal4*). The expression domains of these promoters overlap only in cortex glia and therefore lead to the precise activation of UAS-driven transgenes in cortex glia (Fig. 1; Supplemental Figs. S2M–O, S3). The *CtxGlia-SplitGal4* line therefore allows for precise labeling, manipulation, and exploration of the biology of cortex glial populations in *Drosophila*.

Cortex glia are generated from neural precursors at mid-embryogenesis (Ito et al. 1995; Freeman and Doe 2001). To determine the spatiotemporal dynamics of their morphogenesis, we visualized cortex glia by driving membrane-tagged GFP with *CtxGlia-SplitGal4* and examined their development at selected time points in embryonic, larval, and adult stages. Throughout the study, we used the VNC as a model due to its stereotyped segmentation. Cortex glial cells were born around embryonic stage 12 (Fig. 1A). They sent out processes to envelop neuronal cell bodies in groups or individually by stage 15–16 (Fig. 1B) and infiltrated the entire cortex region of the CNS in the first instar larval stage (L1) (Fig. 1C). *CtxGlia-SplitGal4* labeled cortex glia of the central brain and VNC throughout larval

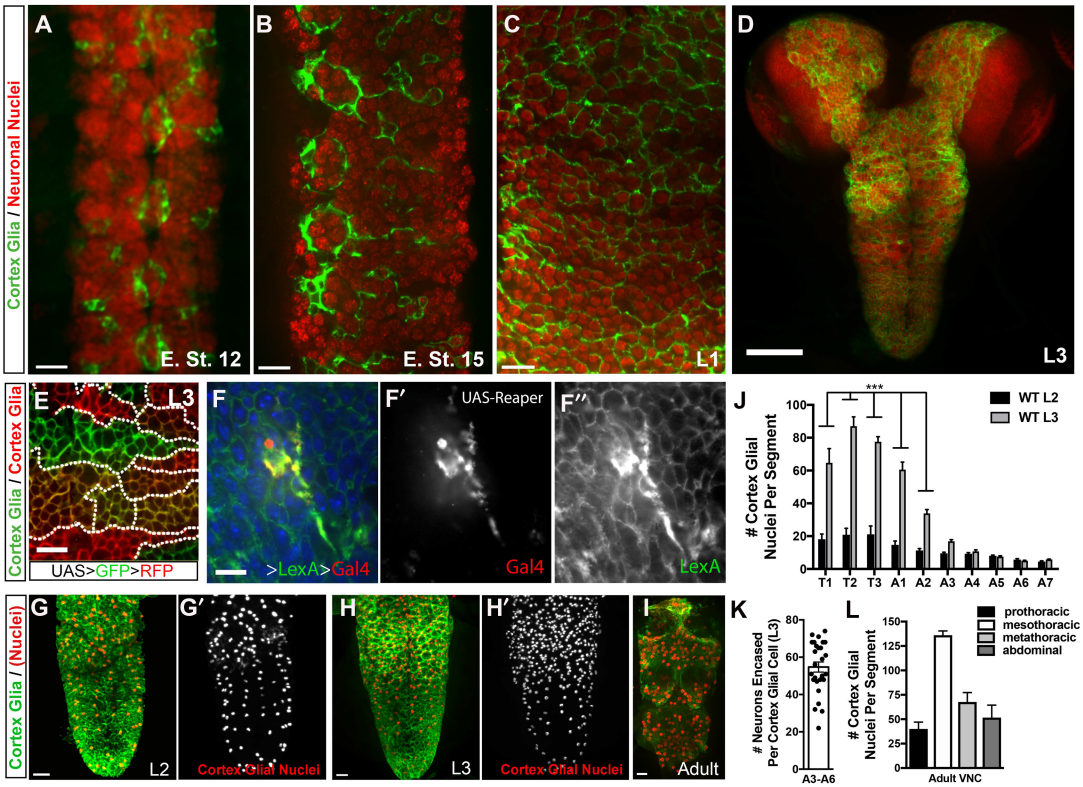

Figure 1. *CtxGlia-SplitGal4* allows for cortex glial-specific labeling and investigation of glia–neuron contacts throughout development. (*A–C*) Cortex glia infiltrate the cortex during embryonic development. Cortex glia are established around embryonic stage 12 (*A*), extend processes to wrap neurons either in groups or individually as embryogenesis proceeds (*B*), and fully infiltrate the CNS around the first instar larval stage (*C*). Cortex glia are labeled with *UAS-CD8GFP* (green; anti-GFP), and neuronal nuclei are stained with anti-Elav (red). (*D*) *CtxGlia-SplitGal4* labels cortex glia in the central brain and VNC, shown here at the third instar larval stage (L3). Bar, 50 µm. (*E*) Stochastic flp-out expression of GFP and RFP reveals that cortex glia form tiled domains with themselves (*GMR54H02-gal4,UAS-CD8>GFP>RFP*). Bar, 10 µm. (*F*) In the presence of flipase activity, *Wrapper932i>LexA>Gal4* stochastically switches from the LexA driver to Gal4. Flp-out clones of cortex glia expressing the cell death gene reaper (*UAS-rpr*), marked by *UAS-CD8Cherry* (red), degenerate from *Reaper* activity. Neighboring control cortex glia that express only *LexAop2-CD8GFP* (green)—without *UAS-rpr* expression—grow to fill in empty space, leaving no unwrapped neurons. Bar, 10 µm. (*G–H′*) Cortex glial nuclei (labeled with *CtxGlia-SplitGal4,UAS-LacZ*^{NLS} and stained with anti-βgal [red]) increase significantly from the second instar larval stage (L2) (*G,–G′*) to L3 larval stage (*H,–H′*), specifically in the thoracic (T1–T3) and first two abdominal (of A1–A7) segments. Bars, 20 µm. (*I*) Adult VNC showing that the cortex glial specificity of *CtxGlia-SplitGal4* remains into adult stages. (*J*) Quantification of the numbers of Elav^{+} nuclei contained in each cortex glial cell from abdominal segments A3–A6 in L3 brains. $n = 27$ cells from 21 clones in 15 brains. (*K*) Quantification of cortex glial nuclei in L2 and L3 brains. $n = 7$ brains per time point. (***) $P < 0.0001$, two-way ANOVA with Sidak's multiple comparison test. (*L*) Quantification of cortex glial nuclei in each segment of the adult VNC. $n = 5$ brains.

development, including late stages (third instar larval stage [L3]) (Fig. 1D). Using a conditional "Flp-out" approach (with UAS-mCD8>GFP>RFP and *repo-FLP*), we found that cortex glia establish self-tiled domains (Fig. 1E) similar to *Drosophila* (Stork et al. 2014) and mammalian astrocytes (Bushong et al. 2004). *repo-FLP* has stochastic activity that can turn on throughout the life of glial cells, which accounts for the resulting green cells (unflipped), red cells (flipped), and yellow cells (flipped cells that have turned on RFP expression but not yet fully degraded GFP). Interestingly, the precise cortex glial spatial domains appeared to be plastic. For example, the ablation of single cortex glial cells (with *UAS-reaper* driven stochastically in flp-out clones of *wrapper932i>LexA>Gal4* using *repoFLP*) resulted in surrounding cortex glia growing in to fill the territory of the ablated cell (Fig. 1F–F″). After testing many such cell ablations, we rarely saw gaps of unwrapped neurons around the red cortex glial debris, suggesting that cortex glia may compete for CNS space during development. To determine whether animals could survive without cortex glia, we selectively ablated cortex glia with *UAS-hid* and *CtxGlia-SplitGal4* (Supplemental Fig. S3). We found that ablation of cortex glia resulted in lethality at early larval stages for most animals, indicating that cortex glia are important for survival.

To quantify populations of cortex glia, *CtxGlia-SplitGal4* was crossed to *UAS-LacZ*^{NLS} and stained with anti-βgal. βgal^{+} nuclei were counted per segment; segments were defined by nc82 staining and morphological demarcations. Cortex glial numbers remained stable throughout development from embryonic stages (Ito et al. 1995) through second instar larva (L2); however,

the number of cortex glial nuclei dramatically increased during L2–L3 stages (Fig. 1G,H). The number of cortex glial nuclei exhibited a threefold to fourfold increase between L2 and L3 stages in the thoracic (T1–T3) and first abdominal (A1–A2) segments (Fig. 1J), possibly in conjunction with late larval neuronal proliferation that occurs in preparation for populating the adult VNC. We next generated cortex glial flp-out clones using *repo-FLP* to examine the morphology and territories of individual cortex glial cells at L3. Single cortex glial cells in the VNC abdominal segments of L3 larva ensheathed an average of 55 neurons, with a range as low as 22 and as high as 74 (Fig. 1K). The morphology and location of cortex glia did not appear to be stereotyped with respect to the number of neuronal cells ensheathed or the precise domain of the CNS covered, suggesting that the establishment of cortex glial domains was stochastic, perhaps being defined through competitive interactions with neighboring cells. The CNS undergoes a significant amount of remodeling during metamorphosis; cortex glia remain labeled by *GMR54H02-Gal4* and *CtxGlia-SplitGal4* through this period and into adult animals (Fig. 1I,L).

Defining the boundaries of cortex glia in the CNS has been difficult based on the nonspecific expression observed in previously described cortex glial driver lines. Using *CtxGlia-SplitGal4*, we found that the entire cortex glial population formed interglial boundaries where they closely abutted other glial subtypes throughout the entire CNS, such as ensheathing and wrapping glia (labeled with *GMR83E12-Gal4,UASCD8Cherry*) as well as astrocytes (labeled with anti-GAT) (Supplemental Fig. S1C–E). While axons and dendrites must pass through the cortex glial network in order to reach the neuropil and wire into synaptic circuits, cortex glia were not previously thought to wrap neurites in the neuropil; however, we found that they extended processes to wrap proximal regions of CNS axon bundles. These bundles consisted of distinct glial layers with ensheathing glia on the outer surface (Supplemental Fig. S1F) as well as cortex glia in direct contact with Futsch$^+$ axons along nerves at the neuropil/cortex interface (Supplemental Fig. S1G). This observation suggests that cortex glia may also play important roles in axon biology.

An RNAi-based screen identifies genes required for cortex glial morphogenesis and identifies cortex glial molecular heterogeneity

To identify signaling pathways regulating cortex glial development and functions, we used *CtxGlia-SplitGal4* to conduct an *RNAi*-based screen of >2300 genes (including transmembrane molecules, kinases, phosphatases, and other types of signaling molecules in the *Drosophila* genome) for those whose knockdown led to defects in cortex glial morphology at L3. Briefly, *CtxGlia-SplitGal4, UASCD8GFP* flies were crossed to each individual Vienna *Drosophila* Resource Center (VDRC) UAS-RNAi line or control lines (w^{1118} or $40D^{UAS}$ KK insertional control line) (Vissers et al. 2016). Crosses were raised at 29°C, and cortex glial morphology of the resulting progeny was assessed through the body wall of live wandering L3 larvae under a fluorescent dissecting microscope. Compared with control brains (Supplemental Fig. S4A,D), we found two general types of morphological disruptions: (1) poor cortex glial infiltration with thin processes remaining (Supplemental Fig. S4B) or (2) the appearance of large globular cortex glia that lack thin processes that infiltrate between neuronal cell bodies (Supplemental Fig. S4C). Furthermore, we found that changes in cortex glial morphology could be classified into four separate spatially defined groups. Specifically, alterations occurred (1) throughout the entire CNS (e.g., *furry* and *syntaxin 5*) (Supplemental Fig. S4E,F, respectively), (2) restricted primarily to the brain lobes (e.g., *connector of kinase to AP-1*) (Supplemental Fig. S4G), (3) restricted primarily to the thoracic segments of the VNC (e.g., *nucleoporin 98-96*) (Supplemental Fig. S4H), or (4) restricted primarily to the abdominal segments (e.g., *CG9702*) (Supplemental Fig. S4I). These spatially restricted differences in cortex glial phenotypes suggest the possibility that cortex glia are heterogeneous among these brain regions. We decided to focus on the globular cortex glial morphology with impaired outgrowth of fine processes in the hope of defining new mechanisms required for cortex glial morphogenesis and interactions with neuronal cell bodies.

Membrane fusion machinery is necessary for the maintenance of cortex glial morphology

Knockdown of multiple individual components of signaling pathways that regulate membrane vesicle fusion and transport led to the striking alteration of cortex glia into a globular morphology where cortex glia failed to wrap most neurons at L3 (Fig. 2A–F). Three related genes that gave rise to this phenotype are (1) α*SNAP* (*soluble NSF* [*N-ethylmalemeide-sensitive factor*] *attachment protein* α), the *Drosophila* homolog of *NAPA*, a gene required for zipping and unzipping SNARE proteins during membrane fusion events (Fig. 2C,D; Supplemental Fig. S7A); (2) αSNAP's catalytic binding partner, *NSF2* (Fig. 2E; Supplemental Fig. S7A; Hanson et al. 1995); and (3) *Syntaxin 5*, a SNARE protein shown previously to directly bind αSNAP (Fig. 2F; Rabouille et al. 1998) that is required for fusion events at the Golgi apparatus in an αSNAP-dependent manner. Phenotypes for each of these genes were confirmed by using additional nonoverlapping RNAi lines (Supplemental Table S1). Cortex glia-specific knockdown of all three genes led to globular cortex glia in 100% of animals at L3. The phenotypes ranged from moderate to severe throughout the brains, with the thoracic segments and brain lobes most severely affected. Because these genes are in the same signaling pathway, we focused on αSNAP for more detailed analysis. To confirm endogenous αSNAP expression in cortex glia, we used a previously characterized anti-αSNAP antibody (Babcock 2004) and found that it overlapped with *CtxGlia-SplitGal4* as well as neurons (Supplemental Fig. S5A). Consistent with the fact that our RNAi lines targeted αSNAP, we observed that αSNAP levels were decreased in cortex glia in knockdown animals (Supplemental Fig. S5B). We next examined the

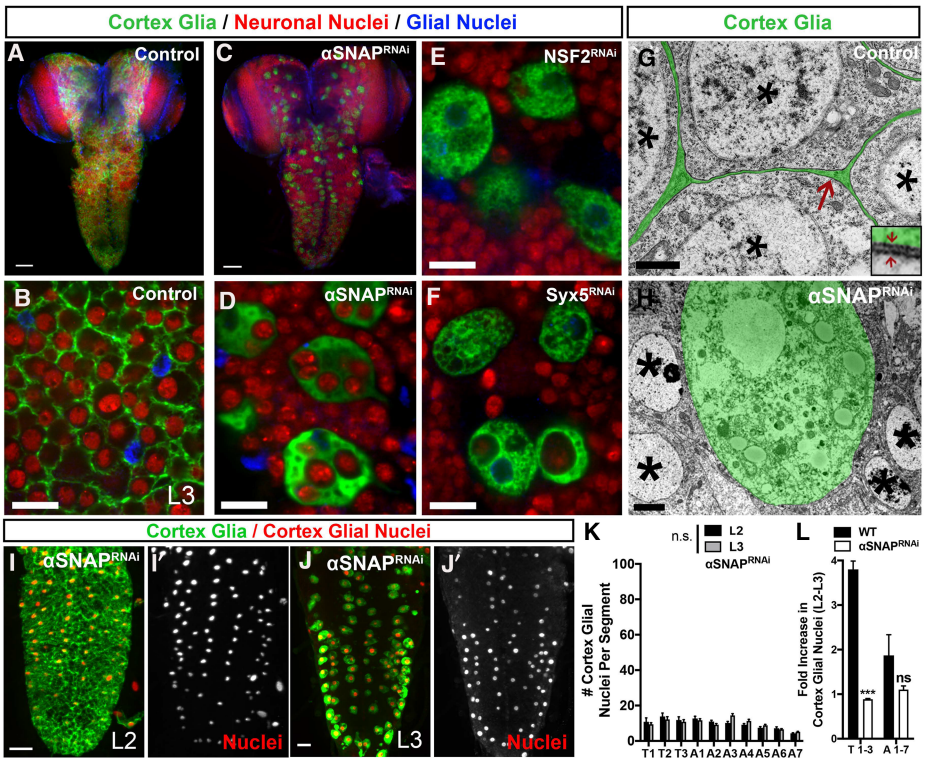

Figure 2. Membrane fusion machinery is necessary for the maintenance of cortex glial morphology. (*A*) Control brain with *CtxGlia-Split-Gal4* driving *UAS-CD8GFP* (anti-GFP, green) stained for neuronal (anti-Elav, red) and glial (anti-repo, blue) nuclei to show normal cortex glia throughout the central brain and VNC. (*B*) High-magnification image of control cortex glia morphology in the VNC. (*C*) Cortex glia expressing RNAi against αSNAP result in globular morphology, leaving many neurons unwrapped by cortex glia. (*D*) High-magnification image of globular cortex glia induced by αSNAP knockdown. (*E*,*F*) Cortex glial RNAi knockdown of αSNAP-binding partners NSF2 (*E*) and Syx5 (*F*) mimics the αSNAP knockdown phenotype. Bars: *A*,*C*, 50 µm; *B*,*D*–*F*, 10 µm. (*G*,*H*) EM of cortex glia pseudocolored in green with neuronal cell bodies outside the glial cell (*). (*G*) Control cortex glia between neuronal cell bodies with processes as thin as 50 nm (*inset* area; indicated by crimson arrow). (*H*) Globular cortex glial cell induced by cortex glia-specific αSNAP^{RNAi} lacks processes between neurons. Bar: *G*,*H*, 1 µm. (*I*,*J*) Without αSNAP, cortex glial nuclei do not increase from L2 (*I*,*I*′) to L3 (*J*,*J*′). Bars, 20 µm. (*K*) Quantification of cortex glial nuclei. (n.s.) Not significant. (*L*) Fold increase from L2 to L3 is compared with controls. $n = 7$ brains each. (***) $P = 0.0002$, two-way ANOVA with Sidak's multiple comparison test.

phenotypic effects of cortex glia-specific knockdown of αSNAP at the electron microscopic level to more rigorously determine whether any fine cortex glial processes remained that could not be detected at the level of light microscopy. In our electron microscopy (EM) analysis, we found that cortex glial processes in control brains could be as thin as 50 nm between neuronal cell bodies (Fig. 2G), and their fine membranes were found abutting nearly all neuronal somata (Fig. 2G, inset). In knockdown conditions, cortex glia were identified based on the large globular structures matching those seen in confocal analysis (Fig. 2H), and we found the cortex glia expressing αSNAP^{RNAi} no longer extended processes between neuronal cell bodies. In an attempt to analyze cortex glia in α*SNAP* mutant animals, we examined a strong hypomorphic allele (α*SNAP*^{G8}) in *trans* to a hypomorphic allele that knocks down ~30%–40% of the αSNAP protein (α*SNAP*^{M4}) (Babcock 2004). However, these *trans*-heterozygous alleles led to animal lethality at L2 and resulted in only partial reduction of αSNAP. Cortex glia in αSNAP$^{G8/M4}$ animals were still labeled by anti-αSNAP antibodies (Fig. 5C), and cortex glial infiltration persisted throughout this time. We suspect that the remaining αSNAP protein expression at L2 is sufficient for normal cortex glial development or that the phenocritical period occurs later in development than L2.

To determine whether the αSNAP^{RNAi} phenotype was a result of defective cell fate specification and early morphogenesis or the maintenance of cortex glial morphology, we examined αSNAP^{RNAi} phenotypes over multiple developmental stages. Cortex glia migrate to their proper stereotyped positions (medial-most [MM], medial [M], ventrolateral [VL], and lateral [L]) during embryonic development (Ito et al. 1995; Akiyama-Oda et al. 1999). Even after constitutive αSNAP^{RNAi} expression throughout embryonic and larval stages, cortex glia migrated to their correct M, MM, VL, and L positions in the embryonic VNC (seen as stripes of nuclei in Fig. 2J) and successfully infiltrated the cortex through the L2 stage. However, cortex glia failed to maintain their morphology from L2 to L3 stages; instead, they retracted their previously established processes and acquired the globular morphology (Fig. 2K).

αSNAP knockdown also affected cortex glial nuclear proliferation at these later developmental stages. Like control brains, the numbers of cortex glial nuclei remained stable from embryonic development through mid-larval stages; however, in contrast to controls (Fig. 1G,H,J), cortex glia with αSNAP knockdown did not increase their numbers from L2 to late L3 (Fig. 2L,M). We conclude that αSNAP is necessary for the maintenance of cortex glial morphology and growth in the developing larval CNS and that disruption of αSNAP function in cortex glia suppresses glial proliferation prior to metamorphosis.

Vesicle fusion machinery is used widely in animals during cellular growth and physiology. It is plausible that the phenotypes that we observed upon manipulation of the vesicle fusion machinery with αSNAP could be indirect, resulting from a general disruption of trafficking. To explore this possibility more deeply, we targeted the entire family of *Drosophila* Rab proteins, which are essential regulators of nearly all types of intracellular vesicle transport. Each Rab is specific to different intracellular compartments and types of vesicle transport, and individual Rab proteins can be targeted selectively with RNAi and/or dominant-negative constructs. We used a collection of lines that endogenously tag all *Drosophila* Rab molecules with YFP so that their expression can be observed under the control of their endogenous promoters (Dunst et al. 2015). We found that most Rabs were endogenously expressed in cortex glia (Fig. 3A,B,D), with the exceptions of Rab3, Rab14, Rab26, Rab27, and RabX4 (Fig. 3C,D). We then assayed all cortex glial-expressed Rabs for roles in maintenance of glial morphology. The majority of the 25 Rabs tested did not alter cortex glial morphology when interrupted by RNAi-mediated knockdown or expression of dominant-negative constructs, suggesting that general disruption of Rab activity or vesicle trafficking is not sufficient to influence cortex glial development. Rather, only dominant-negative expression or RNAi knockdown of Rab1, Rab11, Rab35, and, to a lesser extent, Rab5 mimicked the αSNAP phenotype. As with αSNAP, these animals exhibited normal cortex glia through L2 and developed globular cortex glia by L3 (Fig. 3E–L). Interestingly, these Rabs are engaged in recycling and vesicle secretion (Dunst et al. 2015; Sorvina et al. 2016), suggesting a particularly important role for vesicle secretion/recycling in the context of maintenance of glial morphology.

Disruption of cortex glial morphogenesis leads to aberrant astrocyte overgrowth into the cell cortex region

Cortex glia and astrocytes normally occupy adjacent, largely nonoverlapping domains in the VNC (Supplemental Fig. S1). In control brains, *Drosophila* astrocytes remain restricted to the neuropil region, while cortex glia reside in the cell cortex of the brain (Fig. 4A,F; Supplemental Fig. S1). Unexpectedly, when we examined astrocyte morphology in animals with ablated cortex glia (Fig. 4B) or globular cortex glia induced by α$SNAP^{RNAi}$ expression (Fig. 4C), we found that astrocytes began to infiltrate the cortex region. Although a small number of astrocyte processes were sometimes observed extending short distances into the cortex region of control animals (16.2% of hemisegments and 10.49% ± 2.74% of cortex depth) (Fig. 4A [arrowheads], quantified in D), astrocytic processes inappropriately invaded portions of the cortex region in cortex glial *hid* animals (98.72% of hemisegments and 98.22% ± 1.15% depth of cortex) (Fig. 4B,D) and the majority of segments in cortex glial α$SNAP^{RNAi}$ animals (77.4% of hemisegments and 93.8% ± 6.35% depth of cortex) (Fig. 4C,D). These aberrant glial processes were not due to astrocyte

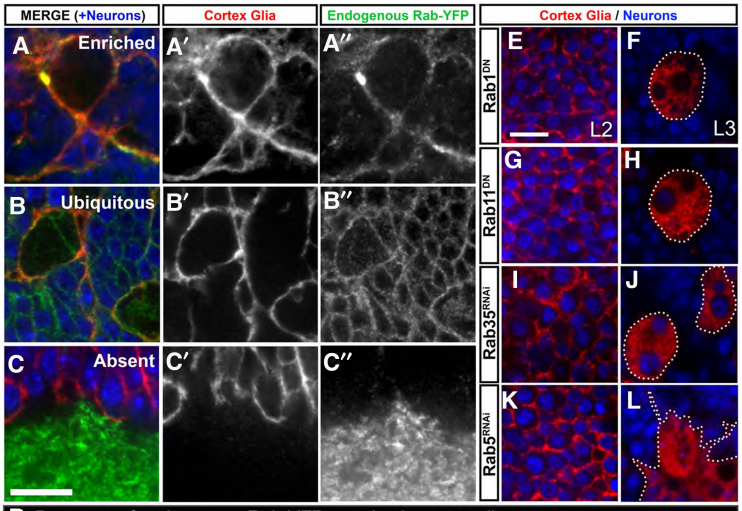

D Presence of endogenous Rab-YFP proteins in cortex glia

Enriched in cortex glia
RabX1 (*A)
Detected in cortex glia as well as other cells
Rab1, Rab2, Rab4, Rab5, Rab6, Rab7, Rab8, Rab9, Rab10, Rab11, Rab14, Rab18, Rab19, Rab21, Rab23, Rab30, Rab32, Rab35 (*B), Rab39, Rab40, RabX5, RabX6
Not detected in cortex glia
Rab3, Rab14, Rab26 (*C), Rab27, RabX4

Figure 3. Disruption of Rab1, Rab5, Rab11, and Rab35 impairs cortex glial morphology. (*A–D*) Using the Rab-YFP collection that expresses YFP-tagged Rab proteins under the control of their endogenous promoter (Dunst et al. 2015), we determined that only RabX1 seems to be enriched in cortex glia (*CtxGlia-SplitGal4,UAS-CD8mCherry*, red) compared with surrounding cells (shown in *A*). (*B*) Most *Drosophila* Rab proteins are present to some extent in cortex glia but also seem to be fairly ubiquitous. For example, Rab35 can be seen in both cortex glia and the neurons they surround. (*C*) A few, such as the example of Rab26, were not found to be expressed in cortex glia. (*D*) Table of the Rab-YFP proteins listed by their expression relative to cortex glia. (*E–L*) Interruption of Rab signaling with RNAi or dominant-negative (DN) constructs only recapitulated the globular cortex glial phenotype, with both dominant-negative and RNAi constructs targeting Rab1 (*E,F*), Rab11 (*G, H*), Rab35 (*I,J*), and, to a lesser extent, Rab5 (*K,L*). Like αSNAP, these defects arise between the L2 (*E,G,I,K*) and L3 (*F,H,J,L*) stages. Bars, 10 µm. The bar for *A–C* is shown in *C*, and the bar for *E–L* is shown in *E*.

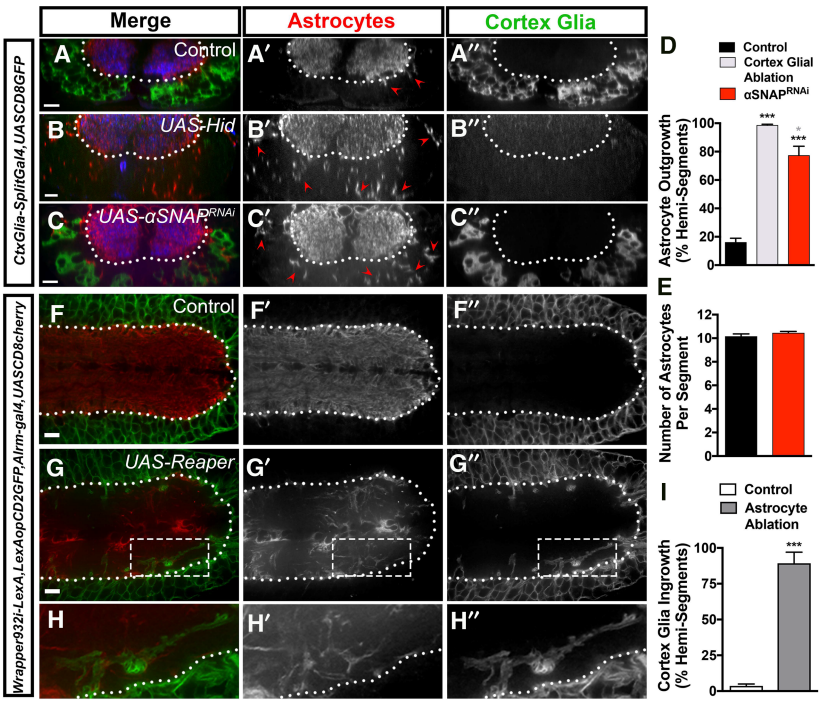

Figure 4. Dysfunctional glia lead to aberrant growth of neighboring glial subtypes. (*A*) Cross-section of control L3 VNC with neuropil-restricted astrocytes (anti-GAT, red; *A′*) and cortex-restricted cortex glia (*CtxGlia-SplitGal4, UAS-CD8GFP* stained with anti-GFP, green; *A″*) costained for synapses (anti-Brp, blue). (*A′*) Arrowheads show small stray astrocytic processes. (*B*,*C*) Cortex glial ablation with *UAS-hid* (*B*) or morphological disruption via *UAS-αSNAP*^{RNAi} (*C*) causes widespread invasion of astrocytes to the cortex (*B′*), whereas synapses remain in the neuropil (*B*), and cortex glia remain in the cortex in αSNAP (*B″*). (*D*) Quantification of the percentage of hemisegments with astrocytes crossing the neuropil–cortex boundary increases from 16.18% of segments in controls ($n = 17$) to 98.72% in *UAS-hid* ($n = 13$) and 77.43% in cortex glia-specific αSNAP^{RNAi} animals ($n = 12$). (*) $P = 0.0227$; (***) $P < 0.0001$, one-way ANOVA with Tukey's multiple comparisons test (with Spz3^{RNAi} shown in Fig. 6E, below). (*E*) Quantification of Prospero^{+} astrocytes shows no difference in astrocyte numbers during the outgrowth events. $n = 7$ control animals; $n = 13$ *SNAP*^{RNAi} animals. (*F*) Longitudinal section of control L3 VNC with neuropil-restricted astrocytes (anti-GAT, red; *F′*) and cortex-restricted cortex glia (*Wrapper932i-LexA,LexAop-CD2GFP* stained with anti-GFP, green; *F″*). (*G*) Astrocyte ablation with *Alrm-Gal4* driving *UAS-reaper* (anti-RFP, red; *G′*) results in cortex glial (anti-GFP, green; *G″*) infiltration into the neuropil. (*H–H″*) Close-up of *inset* in *G–G″*. (*I*) Quantification of the percentage of hemisegments with aberrant cortex glia in the neuropil increases from 3.648% in controls to 89.26% in astrocyte ablated animals. $n = 9$ wild-type ablations; $n = 14$ astrocyte ablations. (***) $P < 0.0001$, unpaired *t*-test. Bars, 10 µm. The dashed line depicts the cortex/neuropil boundary in all images.

proliferation, as the number of astrocytes remained unchanged between control and αSNAP^{RNAi} animals (Fig. 4E). These observations argue that cortex glia normally restrict the growth of astrocyte processes to the neuropil. Interestingly, we also found that genetic ablation of astrocytes using *alrm-Gal4*-driven *UAS-rpr* resulted in a reciprocal aberrant infiltration of cortex glial processes into the neuropil in 89.3% of hemisegments, compared with just 3.6% of controls (Fig. 4F–I). Together, these data indicate that ongoing cortex glia–astrocyte communication is required for each subtype to remain within its appropriate spatial domain. Furthermore, it demonstrates that genetically compromised glia can affect the growth properties of otherwise healthy neighboring glia.

Genetic ablation of glial subtypes such as astrocytes or cortex glia could induce an injury response in the neighboring cells to drive their growth toward physiologically disrupted CNS regions. To date, all injury responses in *Drosophila* (i.e., extension of glial processes to injured neurons) require the engulfment receptor Draper, the homolog of mammalian MEGF10 (Wu et al. 2009). Draper is expressed and functions as an engulfment receptor in both cortex glia and astrocytes to engulf neuronal cell corpses or neurite debris (MacDonald et al. 2006; Kurant et al. 2008; Tasdemir-Yilmaz and Freeman 2014), and this engulfment signaling pathway is conserved in mammals (Wu et al. 2009; Chung et al. 2013). To assay whether cortex glia or astrocytes were growing into neighboring domains to engulf debris in a Draper-dependent manner, we created a *LexAop2*-driven *Draper*^{RNAi} construct to knock down Draper signaling in either cell type. This construct effectively blocked Draper signaling, as it was sufficient to inhibit neuropil invasion by ensheathing glia after axon injury in the adult antennae lobe (a process known to require Draper signaling) (Supplemental Fig. S6A–D). However, in the context of glial overgrowth in the VNC after ablation of neighboring glia, knockdown of Draper in either astrocytes or cortex glia was not sufficient to block the invasion of aberrant glial processes when the adjacent glial subtype was compromised (Supplemental Fig. S6E–H). These data argue that cross-infiltration of spatial domains for cortex glia and astrocytes occurs through Draper-independent mechanisms and is not simply an injury response to dying cells.

Loss of normal cortex glial morphology leads to increased neuronal cell death and behavioral impairment

Even with ingrowth of neighboring astrocytes, many neuronal cell bodies are still devoid of direct glial contact in animals with globular cortex glia (e.g., αSNAP^{RNAi} animals). We exploited this fact to examine how neuronal health and function are affected in vivo when the majority of their cell bodies is not ensheathed by glia. Cortex glia have been proposed to function in regulating ion balance in the neuronal extracellular environment (Melom and Littleton 2013) and to provide an array of trophic and metabolic support to neurons (Buchanan and Benzer 1993;

Volkenhoff et al. 2015). First, we wondered how the abnormal morphology of cortex glia affected physiological functions. Cortex glial processes exhibit dynamic Ca^{2+} signaling events in vivo, which are thought to modulate neuronal activity (Melom and Littleton 2013). Interestingly, we found that prior to the onset of globular morphology, the number of calcium transients over a 90-sec period was reduced from ~14.4 per 400 µm^2 in control cortex glia at L2 compared with 5.1 per 400 µm^2 in L2 cortex glia with αSNAP knockdown (Fig. 5A–C; Supplemental Movie S1). Therefore, loss of αSNAP results in profound changes in cortex glial cellular physiology even before the onset of morphological changes. Given the role of αSNAP in vesicle fusion, it is possible that reduced αSNAP could potentially interfere with the insertion of the membrane-tagged GCaMP5a calcium sensor; however, this is unlikely to be the cause of reduced transients, as similar levels of GFP fluorescence were observed between the two conditions.

We next assayed for behavioral phenotypes to determine whether overall larval CNS physiology was compromised without proper cortex glial infiltration. Larval crawling paths of αSNAP knockdown animals were shorter (Fig. 5D), with a velocity of 5.138 cm/min compared with 6.934 cm/min in controls (Fig. 5E). Interestingly, when longer crawling paths did occur, they were more convoluted than the tracts of control animals. We therefore quantified the linear distance from the starting point to the end point of the crawling path and revealed that this was significantly reduced in knockdown conditions (2.135 cm in αSNAP knockdown compared with 4.382 cm in controls) (Fig. 5F). Finally, we explored how a lack of cortex glial ensheathment of neuronal cell bodies affected neuronal survival in the VNC at L3. We stained for the presence of the cell death marker DCP-1 (cleaved death caspase protein-1) (Akagawa et al. 2015) in control animals and α*SNAP*^{RNAi} animals lacking full cortex glial infiltration. Developmental cell death occurs in control animals, which have, on average, 198.2 cell corpses in the entire VNC; however, αSNAP^{RNAi} animals had an average of 269.9 DCP-1$^+$ cell corpses throughout the VNC, an increase of 36% (Fig. 5G–I). The elevated cell death that we observed in animals lacking cortex glial infiltration argues that cortex glial association with neuronal cell bodies is necessary to promote neuronal survival.

The secreted neurotrophin Spz3 cell-autonomously regulates cortex glial morphology

αSNAP is required for SNARE complex disassembly and functions in vesicle fusion during exocytosis (Supplemental Fig. S7A; Littleton et al. 1998; Xu et al. 1999). Our observation that the disruption of this pathway alters cortex glial morphology highlights an important role for membrane dynamics in maintaining cortex glial morphology. However, this phenotype could result from the pleiotropic effects of loss of vesicle dynamics, including disruption of membrane receptor trafficking, blockade of secreted signaling factors, or simply the lack of insertion of new membranes for cellular expansion. We were particularly interested in whether the effects of α*SNAP* knockdown in cortex glia could at least in part result from reduced exocytosis and protein secretion. In our screen of the 2300 RNAi lines, we also identified Spz3, a cys-knot protein similar to mammalian neurotrophins such as nerve growth factor (NGF) and brain-derived neurotrophic factor (BDNF) (Parker et al. 2001; Zhu et al. 2008; Ballard et al. 2014) that phenocopied many of the effects of loss of αSNAP. First, the developmental time line of phenotypic onset observed with Spz3^{RNAi} in cortex glia matched that

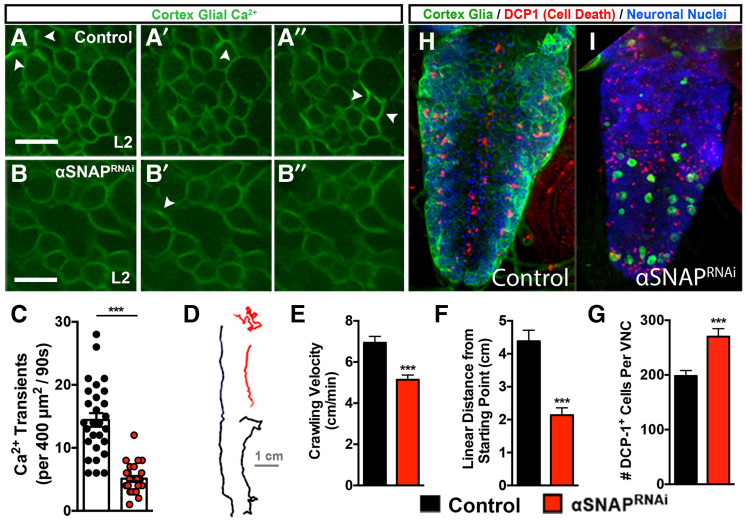

Figure 5. Disruption of cortex glial morphology results in increased neuronal cell death and behavioral impairment. (*A–B″*) Calcium imaging in cortex glia at L2 in control (*A–A″*) and cortex glia-specific αSNAP knockdown (*B–B″*) using *UAS-GCaMP5a* driven by *GMR54H02-Gal4*. Bars, 10 µm. Images shown are at 5-sec intervals. White arrowheads show calcium transients in cortex glial processes. (*C*) Quantification of calcium transients per 400-µm^2 area: control mean = 14.43 transients; αSNAP^{RNAi} = 5.107 transients; $n = 28$ regions of interest; $n = 4$ brains each. (***) $P < 0.0001$, unpaired *t*-test. (*D*) Example traces of larval crawling from control (black) or cortex glial αSNAP^{RNAi} (red) in L3 larva (*CtxGlia-SplitGal4,UAS-CD8GFP* crossed to wild type or *UAS-*α*SNAP*^{RNAi}). (*E*) Quantification of larval crawling speed (centimeters per minute) shows a slight drop from 6.934 cm/min in control animals ($n = 34$) to 5.138 cm/min in αSNAP^{RNAi} animals ($n = 29$). (***) $P < 0.0001$, unpaired *t*-test. (*F*) Quantification of linear distance traveled from the start to the end of the crawling path is reduced from 4.382 cm in control animals ($n = 34$) to 2.135 cm in αSNAP^{RNAi} cortex glia animals ($n = 29$). (***) $P < 0.0001$, unpaired *t*-test. (*G*) DCP1$^+$ (death caspase protein-1-positive) puncta increased from 198.2 in control VNCs to 269.9 in αSNAP^{RNAi} animals. $n = 12$ brains per genotype. (***) $P = 0.001$, one-way ANOVA with Tukey's multiple comparison test (with Spz3^{RNAi} shown in Fig. 6E). (*H,I*) Cell death (anti-DCP-1, red) in control L3 VNC (*H*) or in the presence of globular cortex glia induced by *UAS-*α*SNAP*^{RNAi} (*I*). Cortex glia were visualized with *CtxGlia-SplitGal4* driving *UAS-CD8GFP* (anti-GFP, green) and stained for neuronal nuclei (anti-Elav, blue).

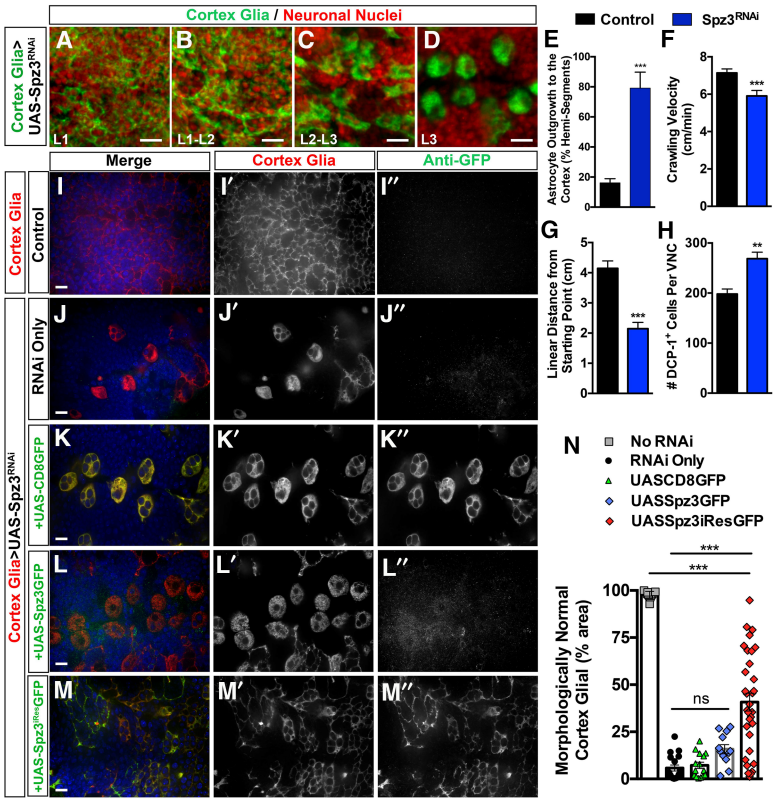

Figure 6. Spz3 cell-autonomously regulates cortex glial morphology. (*A–D*) Knockdown of Spz3 ($Spz3^{RNAi}$) in cortex glia (visualized with *CtxGlia-SplitGal4* driving *UAS-CD8GFP*) resulted in normal development through L1 (*A*) and early L2 (*B*). Progressive morphological disruption occurs between L2 and L3 stages (*C*,*D*). Neuronal nuclei are stained in red (anti-Elav). Bar, 20 µm. (*E*) $Spz3^{RNAi}$ in cortex glia increased aberrant astrocyte outgrowth from 16.18% (n = 17) to 79.17% (n = 9) of hemisegments in the VNC. (***) $P < 0.0001$, one-way ANOVA with Tukey's multiple comparison test (with *hid* and $\alpha SNAP^{RNAi}$ shown in Fig. 4D). (*F*,*G*) $Spz3^{RNAi}$ affected L3 larval crawling with reduced crawling velocity from 7.136 cm/min (n = 49) to 5.908 cm/min (n = 38; [***] P = 0.0008, unpaired t-test; *F*) and decreased linear distance traveled from the starting to the ending points of the path from 4.145 cm in controls (n = 49) to 2.146 cm (n = 38; [***] $P < 0.0001$, unpaired t-test; *G*). (*H*) $DCP1^+$ puncta increased from 198.2 in control VNCs to 268.7 in $Spz3^{RNAi}$ animals. n = 12 brains per genotype. (**) P = 0.0012, one-way ANOVA with Tukey's multiple comparison test (with $\alpha SNAP^{RNAi}$ shown in Fig. 5G). (*I–M″*) *CtxGlia-SplitGal4,UAS-CD8Cherry* crossed to the $40D^{UAS}$ KK insertion control shows normal cortex glial morphology (red) in thoracic segments at L3 (shown in *I–I″*). RNAi targeted to Spz3 results in globular morphology at L3 (*J–J″*) that is not rescued by the addition of *UAS-CD8GFP* (*K–K″*) or *UAS-Spz3GFP* (*L–L″*). (*M–M″*) UAS-driven RNAi-resistant Spz3GFP (*UAS-$Spz3^{iRes}$GFP*) ameliorates cortex glial morphology. Cortex glia are marked with *UAS-CD8Cherry* (anti-RFP, red) and stained for rescue constructs (anti-GFP, green) and neuronal nuclei (anti-Elav, blue). Bar, 10 µm. (*N*) Quantification of the area (from T2–T3 segments) covered by morphologically normal cortex glia reveals 97.8% in control (n = 13 brains), 5.8% in RNAi only (n = 18 brains), 7.2% in cortex glia expressing CD8GFP (n = 15 brains), 15.8% in cortex glia expressing Spz3GFP (n = 12 brains), and 40.76% in cortex glia expressing Spz3iResGFP (n = 32 brains). (***) $P < 0.0003$; (n.s.) $P > 0.49$, one-way ANOVA with Tukey's post hoc test.

of α*SNAP* knockdown (Fig. 6A–D). In addition, globular cortex glia resulting from $Spz3^{RNAi}$ also increased aberrant astrocyte outgrowth (from 16.18% to 79.17%) (Fig. 6E), reduced larval crawling velocity (from 7.136 cm/min to 5.908 cm/min) (Fig. 6F), decreased directional persistence (from 4.145 cm in controls to 2.146 cm) (Fig. 6G), and increased neuronal cell death (to 268.7 $DCP\text{-}1^+$ puncta per VNC) (Fig. 6H). Compared with a VDRC RNAi insertional control in which there is 97.8% coverage with morphologically normal cortex glia (Fig. 6I,N), knockdown of Spz3 resulted in very little remaining normal cortex glial morphology and infiltration (5.8%) (Fig. 6J,N).

To confirm that this result was due to the depletion of Spz3, we assayed cortex glial morphology in $Spz3^P$ mutants (a *P*-element insertion resulting in a strong hypomorphic allele of Spz3) (Ballard et al. 2014) as well as the ability of an RNAi-insensitive Spz3 construct (*UAS-$Spz3^{iRes}$GFP*) to autonomously rescue cortex glial morphology in the presence of $Spz3^{RNAi}$. $Spz3^P$ homozygous animals die at L1. We found that the number of affected cortex glia in the VNC of these early L1 $Spz3^P$ animals as well as the severity of morphological defects were significantly increased in homozygous animals compared with heterozygous controls. These defects were attenuated in homozygous animals with cortex glial expression of Spz3GFP (Supplemental Fig. S8A–C,G,H). Cortex glial morphology in $Spz3^P$ L1 animals was often swollen, with some thin processes remaining rather than completely globular. Interestingly, small areas lacking neurons were found in the cortices of homozygous $Spz3^P$ VNCs. These pockets were reminiscent of the size and shape of the neuronal voids created by globular cortex glia seen with RNAi. While the number of voids was not changed with the addition of Spz3GFP, the size of the voids was reduced in the presence of cortex glial Spz3GFP expression (Supplemental Fig. S8D,E,I,J). Due to the early lethality of $Spz3^P$ homozygous animals, we could not assess whether these swollen cortex glia would still infiltrate normally if allowed to develop further. $Spz3^P$ is viable at least through larval stages in *trans* to Df^{BSC142} (a deficiency uncovering *Spz3*), allowing us to assess cortex glial development in these animals at later developmental time points. These cortex glia infiltrate the cortex normally through L2 and exhibit morphological defects only at L3, following the same time line of morphological defects as seen with RNAi (Supplemental Fig. S8K–O). These data argue that the timing of cortex glial defects is not due to delayed onset of RNAi expression or knockdown efficiency but rather developmental mechanisms. For rescue at later larval stages and to focus on cortex glia-specific effects of reduced Spz3, we compared phenotypes of cortex glial coverage in L3 animals with

Spz3^{RNAi} and either (1) *UAS-CD8GFP* (7.2%) (Fig. 6K,N), (2) a *UAS-Spz3GFP* construct that was not protected from RNAi knockdown (15.8%) (Fig. 6L,N), or (3) the RNAi-resistant *UAS-Spz3^{iRes}GFP* construct (40.76%) (Fig. 6M,N). Neither *UAS-CD8GFP* nor *UAS-Spz3GFP* was able to significantly rescue Spz3^{RNAi}-induced globular cortex glial phenotypes. The only construct able to significantly rescue cortex glial morphology was the RNAi-resistant *UAS-Spz3^{iRes}GFP* (Fig. 6N). This rescue varied from brain to brain, likely due to differences in expression level from cell to cell, which appeared to be stochastic based on levels of GFP (Fig. 6M; Supplemental Fig. S7E,F). The loss of Spz3GFP expression in the presence of *Spz3^{RNAi}* confirms that the *Spz3^{RNAi}* construct targets *Spz3* (Supplemental Fig. S7C,D); moreover, the persistence of Spz3^{iRes}GFP expression demonstrates its RNAi resistance (Supplemental Fig. S7E,F). The cell-autonomous rescue from cortex glia further supports the notion that Spz3 functions via an autocrine signaling mechanism for the regulation of cortex glial growth and maintenance.

Spz family proteins and mammalian neurotrophins have been shown to be secreted proteins that can act over varying distances to induce signaling events in target cells (Parker et al. 2001; Zhu et al. 2008; McIlroy et al. 2013; Egervari et al. 2015; Harward et al. 2016). To test whether Spz3 is also secreted, we transfected S2 cells with Spz3GFP, separated the cells from their conditioned media, and probed both for Spz3 expression (Supplemental Fig. S7B). Compared with nontransfected controls, we found that full-length Spz3GFP protein was present at ~110 kDa only in the transfected S2 cells. We identified smaller bands present only in the conditioned media of the transfected cells that were consistent with the size of the cleaved secreted cys-knot domains of other Spz family proteins (~50–60 kDa, including the 27-kDa GFP) (McIlroy et al. 2013).

We next examined the extent to which expression of Spz3 could rescue morphological phenotypes at differing distances from cortex glia in vivo. We assayed for rescue of cortex glial morphology by expression of Spz3 from astrocytes or neurons in a genetic background where Spz3 was depleted from cortex glia by RNAi. We found that Spz3GFP expression from astrocytes was not sufficient to rescue cortex glia morphology when Spz3^{RNAi} was expressed in cortex glia (Supplemental Fig. S9). This argues that Spz3 cannot signal from the neuropil to the cortex —a distance of <50 µm—in sufficient quantities to affect cortex glial morphology. Despite the fact that Spz3^{RNAi} in cortex glia causes compensatory outgrowth of astrocyte processes into the cortex and therefore might reduce the distance of diffusion, astrocyte spz3GFP expression is not able to rescue the cortex glia defects. We suspect that this is due to the availability of astrocyte processes: Even when astrocytic processes invaded the cortex, the majority of the cortex still lacked astrocyte processes (Supplemental Fig. S9C″). This is consistent with the notion that Spz3 acts at a very short range. In accordance with this, we found that Spz3 expression in neurons (which form much closer and more robust contacts with cortex glial cells) had a significant rescuing effect on cortex glial morphology (Fig. 7). In thoracic segments of control brains at L3 (Fig. 7A,F), infiltration of cortex glial processes was normal in ~94% of the measured brain area, while knockdown of Spz3 (Fig. 7B,F) led to only 2.7% of the area covered by normal cortex glial morphology. Expression of CD8GFP in neurons had no significant effect on cortex glial morphology (Fig. 7C,F). In contrast, Spz3GFP expression from neurons partially restored cortex glial infiltration to an average of 23.3% total coverage (Fig. 7D–F). We suspected that this partial rescue is in part due to sparse neuronal expression of Nsyb-QF2 in the L3 VNC (Fig. 7A,D). Indeed, on closer inspection, we noticed that expression of Spz3GFP predominantly rescued morphology in cortex glia bordering or in close proximity to neurons expressing Spz3GFP (Fig. 7E). Neurons that did not express significant levels of Spz3GFP largely lacked cortex glia ensheathment. Moreover, local expression of neuronal Spz3GFP was also able to rescue the cortex glial morphology after αSNAP knockdown (Fig. 7G,H), arguing that reduced Spz3 secretion is one of the primary effects of removing αSNAP. The fact that adjacent neuronal cell bodies are differentially ensheathed based on their expression of Spz3 further highlights the local nature of Spz3 signaling in driving cortex glial ensheathment of neuronal cell bodies.

Together, our data support a model in which Spz3 acts cell-autonomously to maintain cortex glial morphology and promotes continued cortex glial ensheathment of neuronal cell bodies in the CNS. In addition, we show that maintenance of these contacts is essential for normal neuronal function, survival, and, ultimately, animal behavior.

Discussion

All major glial subtypes in the mammalian CNS make direct contact with neuronal cell bodies, and the vast majority of neuronal cell bodies is associated with glia. However, the detailed study of neuron–glia physiological functions at neuronal cell bodies in vivo has been hindered by the complexity of neuron–glia architecture. For instance, in mammals, a single astrocyte generally associates with many neuronal cell bodies and the entire local synaptic network, consisting of many thousands of synapses. Therefore, directly manipulating interactions at only synapses or the cell body is challenging, and parsing individual physiological functions is difficult without a detailed understanding of the signaling mechanisms selective to each location. Furthermore, the lack of genetic tools to target glia that associate only with cell bodies (e.g., peripheral satellite glia) has precluded the advancement of such efforts.

In this study, we explored the biology of *Drosophila* cortex glial cells, whose processes associate primarily with neuronal cell bodies, but not synapses, to overcome these limitations. We generated and characterized a number of new tools that allow for the specific targeting and manipulation of cortex glia in vivo and used these tools to characterize their development and functional interactions

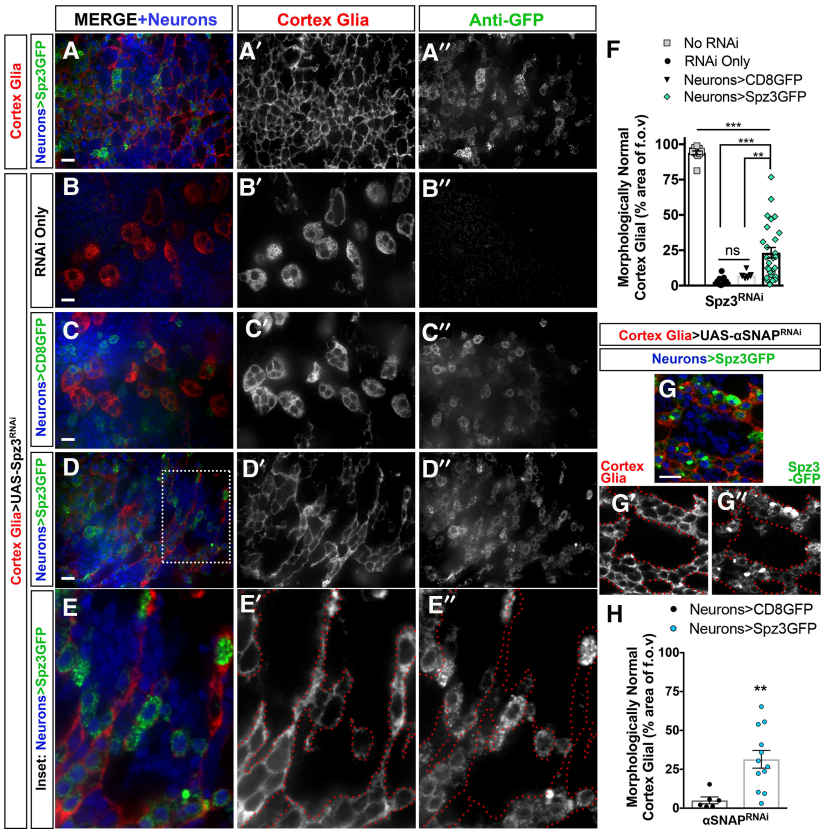

Figure 7. Ectopic neuronal expression of Spz3 can locally regulate cortex glial morphology. (*A*) *CtxGlia-SplitGal4* expressing *UAS-CD8Cherry* with *Nsyb-QF* driving expression of *QUAS-Spz3GFP* in a subset of neurons driven by *Nsyb-QF2* results in relatively normal cortex glial morphology (red) at L3. (*B–E*) $Spz3^{RNAi}$ in cortex glia results in globular morphology at L3 (*B–B″*) that is not rescued by *QUAS-CD8GFP* in neurons (*C–C″*). (*D–D″*) Expression of *QUAS-Spz3GFP* in neurons can ameliorate cortex glial morphology in areas close to Spz3-expressing neurons. (*E*) Close-up of the *inset* in *D* demonstrating rescue of cortex glia along Spz3GFP-expressing neurons (the red line outlines cortex glial processes). Cortex glia are marked with *UAS-CD8Cherry* (anti-RFP, red), neurons expressing QF-driven CD8GFP or Spz3GFP for rescue constructs are shown in green (stained with anti-GFP), and all neuronal nuclei are shown in blue (stained with anti-Elav). (*F*) Quantification of the area (thoracic segments) covered by morphologically normal cortex glia reveals 94.0% in control ($n = 12$ brains), 2.7% in RNAi only ($n = 13$ brains), 7.2% in brains with neurons expressing CD8GFP ($n = 7$ brains), and 23.26% in brains expressing Spz3GFP ($n = 28$ brains). (**) $P = 0.0194$; (***) $P < 0.0003$; (ns) $P > 0.40$, one-way ANOVA with Tukey's post hoc test. (*G–G″*) Expression of *QUAS-Spz3GFP* rescues cortex glial morphology caused by $\alpha SNAP^{RNAi}$ near Spz3-expressing neurons. (*H*) Quantification of neuronal Spz3 rescue of cortex glial coverage in cortex glia driving $\alpha SNAP^{RNAi}$. $n = 6$; $n = 12$, respectively. (**) $P = 0.0057$, unpaired *t*-test. Bars, 10 µm.

with other glial subtypes and neurons. We showed that cortex glia tile with each other and astrocytes, establishing unique spatial domains. Additionally, our results show that the disruption of vesicular fusion, recycling, and secretion leads to a loss of complex cortex glial morphology. Altered cortex glial morphology and signaling had wide-ranging consequences on the CNS, such as aberrant invasion of neighboring astrocyte processes into the cortex region, increased neuronal cell death, and behavioral impairment. Finally, we show that a key factor regulating these events is Spz3, a secreted neurotrophin-like molecule. Spz3 functions autonomously in cortex glia and, based on our rescue experiments in both cortex glia and neurons, appears to act very locally—sometimes over a distance of only a few cell diameters—to modulate maintenance of cortex glial morphology and association with neuronal cell bodies.

Glia maintain interactions with neuronal cell bodies throughout development

Our *CtxGlia-SplitGal4* driver is highly specific in its labeling of cortex glia at all developmental stages. We used this driver to begin to explore basic questions in cortex glial morphogenesis. While it was thought previously that cortex glial processes did not enter the neuropil, we found that cortex glia in fact extend processes a short distance on proximal nerve bundles as they extend into the neuropil; however, we found no evidence for association with synapses. At neuronal cell bodies, we found that cortex glia rapidly invade between neurons almost immediately after they are born in the embryo. This is mechanistically distinct from the larval brain, where cortex glia have been reported to wrap neuroblasts and their newborn progeny in clusters of 15–20 neurons and then later slowly fill in to individually wrap neurons as they mature (Dumstrei et al. 2003). It therefore appears that cortex glia may engage stage- or context-specific programs for ensheathment of neuronal cell bodies.

Cortex glia have been shown to proliferate in the brain lobes based on β-gal staining of nuclei (Avet-Rochex et al. 2012). We also observed increases in nuclear number during mid–late larval stages; however, we are uncertain whether this is due to proliferation or, potentially, endomitosis (the replication of DNA without cell division) (Orr-Weaver 2015). SPGs are multinucleated cells that undergo endoreplication to increase the number of nuclei per cell during larval stages (Unhavaithaya and Orr-Weaver 2012). Although we made extensive attempts, we were unable to reliably generate MARCM (mosaic analysis with a repressible cell marker) clones in VNC cortex glia, although MARCM clone generation in other glial cell types is straightforward (Awasaki et al. 2008; Stork et al. 2014). It is unclear why this is the case. MARCM clone induction relies on the removal of the Gal4 suppressor Gal80 during mitotic recombination (Lee and Luo

1999). One possibility is that cortex glia are multinucleated cells, which would explain the lack of MARCM clone production. In a multinucleated cell, even if some of the recombination events result in the removal of Gal80 from one nucleus, other nuclei in the same cell could retain Gal80 and repress Gal4 function. Such issues with MARCM clone production have been reported by others: Cortex glia and SPGs were rarely labeled when MARCM clones were induced during larval stages (Awasaki et al. 2008).

Cortex glia form homotypic contacts with themselves and heterotypic contacts with astrocytes to establish unique spatial domains that restrict glial growth

It is well established that mature astrocytes tile to form domain boundaries with neighboring cells of the same glial subtype (Bushong et al. 2004; Stork et al. 2014). Here, we demonstrated that cortex glia also exhibit self-tiling behavior. The maintenance of these boundaries appears to be an active process, as was the case with *Drosophila* astrocytes (Stork et al. 2014). The ablation of a single cortex glial cell allows surrounding cortex glia to grow into the domain of the dying cortex glial cell, presumably to ensure the complete ensheathment of neuronal cell bodies. Whether glia of different subtypes similarly tile with cortex glia in a heterotypic manner was not known. We found that cortex glial cells and astrocytes also communicate with one another and help restrict each other's domains of growth. This is reminiscent of cell–cell interactions at the motor exit point transition zone (MEP TZ) at the CNS/peripheral nervous system boundary of the vertebrate spinal cord, where radial glial cells restrict the outgrowth of peripheral glia into the spinal cord, and ablation of radial glial cells leads to the migration of peripheral glia across the MEP TZ boundary (Smith et al. 2016). The aberrant outgrowth of astrocytic processes in the presence of globular cortex glia or the converse growth of cortex glia into the neuropil after astrocyte ablation demonstrates that there is ongoing communication between these subtypes in vivo. This observation indicates that the spatial domains that glia occupy in the CNS are not defined solely by an affinity for that domain (e.g., an attraction of astrocytes to synapses in the *Drosophila* neuropil) but instead are actively delimited by neighboring repulsive interactions with neighboring populations of glia cells. Whether these glia cross-infiltrate in response to factors from the manipulated glial cells or perhaps stress signals from neurons in the domain of glia ablation awaits further investigation.

Cortex glia require ongoing vesicle fusion, recycling, and Spz3 signaling to maintain their morphology

Vesicle fusion is achieved by the pairing of *trans*-SNARE complexes necessary to bring vesicles together with their target membranes (Supplemental Fig. S7A). αSNAP is involved in all aspects of vesicle fusion events, as it is necessary for the unclasping of *cis*-SNARE complexes prior to *trans*-SNARE binding (Littleton et al. 1998). The knockdown of αSNAP or its ATPase-binding partner, NSF2, is predicted to disrupt vesicle fusion events such as exocytosis (Littleton et al. 1998; Xu et al. 1999; Babcock 2004). Mammalian glial cells have been proposed to rely on SNARE-dependent mechanisms for Ca^{2+}-dependent exocytosis in gliotransmission (Bezzi et al. 2004). That we observed a dramatic change in cortex glial Ca^{2+} transients might be explained by a role for SNARE-dependent mechanisms in maintaining Ca^{2+}-dependent release of glial factors by a similar mechanism at neuronal cell bodies. Perhaps the highly elaborate nature of cortex glial morphology renders these cells particularly sensitive to perturbations in signaling and results in changes in morphogenesis or morphological maintenance.

The requirement of αSNAP in vesicle fusion in exocytosis led us to search for a secreted molecule that mimicked the effects of the cortex glia-specific knockdown of αSNAP on cortex glial morphology. Our identification of Spz3 as a key signaling factor in cortex glial morphogenesis that phenocopies all defects associated with the loss of SNARE-dependent events in cortex glia argues strongly that there are specific factors released to promote the development and maintenance of cortex glial structure and neuronal association. Spz3 is a member of the *Drosophila* neurotrophin-like Spz family (Parker et al. 2001; Zhu et al. 2008; Ballard et al. 2014). The founding family member (Spz) as well as two other members (Spz2 and Spz5; *Drosophila* neurotrophins 1 and 2, respectively) have been shown to regulate cell death and axon targeting in the embryonic CNS (Zhu et al. 2008; Sutcliffe et al. 2013); however, whether these genes regulate glial growth had not been explored. We show a direct role for Spz3 in regulating cortex glial growth and morphological maintenance and implicate cortex glial Spz3 signaling in neuronal survival. Whether the increased neuronal cell death arises from a direct loss of Spz3 signaling from cortex glia to neurons or the disruption of cortex glial neuronal ensheathment caused by the loss of autonomous signaling is unclear. In either case, cortex glial Spz3 signaling is essential for neuron health.

Cortex glia do not associate with the synaptic neuropil and therefore provide the opportunity to explore glial functions selectively at neuronal cell bodies. We found that early elimination of cortex glia causes early animal lethality and that loss of cortex glial ensheathment of neuronal cell bodies at later stages results in increased neuronal cell death and behavioral impairment. The physiological basis of this circuit dysfunction is difficult to determine. Cortex glia are predicted to serve many roles in the *Drosophila* CNS, a lack of any of which could explain these phenotypes. First, without cortex glia, neurons might not receive the metabolic or ionic balance support necessary for neuronal survival and function (Melom and Littleton 2013; Volkenhoff et al. 2015). Second, globular cortex glia likely do not clear neuronal cell corpses or other cellular debris, which is one of their normal functions (Kurant et al. 2008), thereby resulting in accumulation of excessive neuronal debris that could lead to circuit dysfunction. In mammals, insufficient microglial clearance of cell corpses or synaptic elements during development

is associated with altered pruning (Kim et al. 2017), a mechanism implicated in autism spectrum disorders. The observed defects in animal behavior could also arise from the direct modulation of neural activity and circuitry by cortex glia. Cortex glial Ca^{2+} signaling events have been proposed to regulate neural physiology (Melom and Littleton 2013), and knockdown of αSNAP severely disrupted cortex glial Ca^{2+} signaling.

Cortex glial invasive growth and morphological elaboration are regulated by local Spz3 signaling

One particularly notable finding is that very local signaling appears to regulate maintenance of cortex glial morphology and association with neuronal cell bodies. The rescue of cortex glial morphology often occurred in cortex glia in close proximity to neurons ectopically expressing Spz3 and not their immediate neighbors, arguing that Spz3 can promote cortex glial membrane expansion over only a short distance (i.e., less than one cell diameter). Mammalian neurotrophins also signal over very short distances. Evidence from astrocytes studies in vitro suggests that vascular endothelial growth factor (VEGF) is released from astrocytes in a directional manner, with subsequent accumulation in the extracellular matrix at adhesion sites for spatially restricted signaling (Egervari et al. 2015). This study further suggested that VEGF secretion occurs close to its receptor, VEGFR2, for localized signaling and that the receptor undergoes constant endocytosis and recycling during signaling events. Furthermore, BDNF has been shown recently to signal in an autocrine fashion from single dendritic spines back onto themselves to regulate their own structural and functional plasticity (Harward et al. 2016; Hedrick et al. 2016). Interestingly, the BDNF receptor TrkB has been shown to function in a Rab11-dependent mechanism (one of the Rabs that we found to regulate cortex glial morphology), where it is retained in dendrites to increase local BDNF signaling and control dendritic arborization (Lazo et al. 2013). A similar mechanism could be involved in cortex glial growth and maintenance, with local autocrine signaling of Spz3 to maintain cortex glial morphology and function.

Cortex glia are some of the most invasive cells in the *Drosophila* CNS. They grow from compact cells to form an elaborate network of extensive thin processes that cover the entire CNS in <24 h (Fig. 1). The genetic accessibility of these cells in an in vivo system makes cortex glia an excellent model to understand neuron–glia interactions at the neuronal soma in both normal physiology and disease models as well as for the study of glial invasive cell behavior—a topic of extremely high interest in diseases such as glioma. Additionally, the entire network of cortex glial cells throughout the brain has been shown to react in a coordinated manner in response to localized injury (Doherty et al. 2014). This is reminiscent of the satellite glial pain and injury response in peripheral sensory ganglia, making cortex glia a candidate population in which to study network responses and explore their roles in sensory signaling in vivo.

Materials and methods

Fly strains

Drosophila melanogaster were raised at 29°C unless noted otherwise. This temperature was chosen to increase Gal4/UAS-RNAi expression rather than coexpressing *UAS-dicer2*; however, phenotypes were the same at 25°C (Supplemental Fig. S4J,K). The following transgenes were generated for this study: *CtxGlia-SplitGal4*, *Wrapper932i-LexA*, *Wrapper932i-Gal80*, *Wrapper932i >LexA>Gal4*, *UAS-Spz3GFP*, *UAS-Spz3iResGFP*, *QUAS-Spz3GFP*, *LexAop2Spz3GFP*, and *LexAop2DraperRNAi* (see the Supplemental Material for cloning strategies). The following previously made *D. melanogaster* transgenes were used in this study (see the Supplemental Material for references and Bloomington/VDRC stock numbers): *GMR54H02-Gal4*, *nrv2-Gal4*, *NP2222-Gal4*, *NP577-Gal4*, *repo-Gal4*, *GMR83E12-Gal4*, *alrm-Gal4*, *GMR25H07-LexA*, *UAS-CD8*::GFP, *UAS-αSNAP^{RNAi}*, *UAS-NSF2^{RNAi}*, *UAS-Syx^{RNAi}*, *UAS-Spz3^{RNAi}*, *Spz3^{P}* (*Spz3^{EY06670}*), *Df^{BSC142}* [*DF(2L)BSC142*], *αSNAP^{G8}*, *αSNAP^{M4}*, *LexAop2-mCD8::GFP*, *LexAop-rCD2::GFP*, *UAS-lacZ-NLS*, *nSyb-QF2*, *QUAS-CD8-GFP*, *UAS-reaper*, UAS-*hid^{ALA5}*, *UAS-CD8-mCherry*, *repoFLP$^{6-2}$*, *UAS-CD8>GFP>RFP*, *UAS-GCaMP5a*, and *alrm-LexA::GAD*. A list of endogenously tagged Rab-YFP lines, dominant-negative Rab lines, and all other RNAi lines used in this study is in Supplemental Table 2.

Immunohistochemistry and imaging

Larval CNSs were dissected in PBS, fixed in ice-cold 100% methanol for 5 min before washing with PTX (PBS + 0.1% Triton-X), and subsequently stained overnight at 4°C with antibodies in PTX. Adult heads were decapitated, fixed for 20 min in 4% formaldehyde/PTX, washed in PTX, and stained. Embryos were dechorionated with 50% bleach for 3 min prior to fixation with 4% formaldehyde/PEMFA (100 mM PIPES at pH 6.9, 2 mM EGTA, 1 mM $MgSO_4$) for 25 min, vortexed, and washed in methanol prior to staining. The following primary antibodies were used: chicken anti-GFP (1:1000; Abcam), rabbit anti-dsRed (1:500; Clontech), rat anti-mCherry (1:500; Molecular Probes), rat anti-Elav (1:100; Developmental Studies Hybridoma Bank [DSHB], 7E8A10), rabbit anti-Gat (1:3500) (Stork et al. 2014), mouse anti-Repo (1:58; D12), rabbit anti-DCP-1 (1:200; Cell Signaling), rabbit anti-β-Gal (1:3000; Promega), goat anti-HRP conjugated to Cy5 (1:500; Jackson ImmunoResearch Laboratories), rabbit anti-SNAP (1:1000) (Babcock 2004), rabbit anti-Draper (1:400; after preabsorption with *yw* embryos overnight) (Freeman et al. 2003), mouse anti-Bruchpilot (1:20; DSHB, nc82), and mouse anti-futsch (1:400; DSHB, 22C10). Primary antibodies were detected with the appropriate goat or donkey secondary antibodies conjugated to Dylight488 (chicken [103-005-155]), Cy3 (rabbit [711-165-152], mouse [715-165-151], and rat [712-175-153]), or Cy5 (rabbit [711-175-152], mouse [715-175-151], and rat [712-175-150]) from Jackson ImmunoResearch. Antibodies were used to enhance endogenous fluorescent protein expression. Samples were mounted in VectaShield reagent (Vector Laboratories) and imaged on an Innovative Imaging Innovations (3I) spinning-disc confocal microscope equipped with a Yokogawa CSX-X1 scan head.

Live calcium imaging

Calcium imaging was performed in live L2 larvae. *GMR54H02-Gal4,UAS-myr-GCaMP5a/+* or αSNAP^{RNAi}/+;*GMR54H02-Gal4,UAS-myr-GCaMP5a/+* larvae were mounted in Halocarbon Oil 27 between coverslips and glass slides to immobilize the

animals, and cortex glial calcium activity was imaged through the cuticles of intact larvae. Imaging was performed on an Innovative Imaging Innovations (3I) spinning-disc confocal microscope equipped with a Yokogawa CSX-X1 scan head.

Larval crawling behavior

Larval crawling velocity was performed and measured as described previously (Stork et al. 2014), with the exception that flies were raised at 29°C. The linear distance traveled was measured as the distance between the starting and ending points to determine straight line persistent crawling behavior.

Transmission EM (TEM)

TEM was conducted on the CNSs of L3 larvae in conjunction with the University of Massachusetts Medical School Electron Microscopy Core Facility as described previously (Tasdemir-Yilmaz and Freeman 2014).

Analysis and statistics

ImageJ was used for all quantifications. The number of neurons wrapped within one cortex glial cell was measured from *Z*-series containing entire cortex glial cells of abdominal segments A3–A6. The number of neurons within each clone was counted and divided by the number of repo$^+$ nuclei in each clone. The majority of clones used for quantification was single cells; however, of the three quantified clones containing more than one cortex glial cell, one contained two cells, one contained three cells, and one consisted of four cells. Calcium signaling transients were calculated by choosing 400-μm^2 areas in a single *Z*-plane and counting the number of calcium transients that occurred within that area during 90 sec. Cortex glial rescue was assessed from single *Z*-plane images taken with a 63× objective (134.4 μm × 102.4 μm) in the region of the thoracic segments of L3 VNCs that contained the cell bodies of the MM cortex glia. The area containing normal cortex glial morphology was measured, and values were reported as the percentage of the field of view containing morphologically normal cortex glia; therefore, the area containing globular was not counted in any image. Error bars in all graphs indicate ± SEM. Statistical significance was calculated with Graphpad Prism 6 software by statistical analysis with either a Student's *t*-test for comparison between pairs or an ANOVA with the appropriate post hoc test for comparing more than two sets of data. All larval crawling was measured and quantified together and therefore analyzed in a common ANOVA with Tukey's post hoc test; however, the results are displayed in separate graphs for presentation.

Acknowledgments

We are grateful to the Vienna *Drosophila* RNAi Center and the Bloomington Stock Center for providing fly stocks. Leo Pallanck generously shared the αSNAP antibody (Babcock 2004). We thank Lara Strittmatter and the University of Massachusetts Medical School Electron Microscopy Core Facility for assistance with TEM experiments (supported by award no. S10RR027897 from the National Center For Research Resources). We are appreciative to Elaine Chang for assistance with the RNAi screen; Dori Schafer, Megan Corty, and Tobias Stork for critical reading of the manuscript; and all members of the Freeman laboratory for engaging discussions and suggestions throughout the project. This work was supported by National Institute of Neurological Disorders and Stroke (R01NS053538 to M.R.F., and F32NS089203 to J.C.C.-B.) and an American Cancer Society Post-doctoral Fellowship (PF-14-169-01-CSM to J.C.C.-B.). M.R.F. was an Investigator with the Howard Hughes Medical Institute during a portion of this study.

References

Akagawa H, Hara Y, Togane Y, Iwabuchi K, Hiraoka T, Tsujimura H. 2015. The role of the effector caspases drICE and dcp-1 for cell death and corpse clearance in the developing optic lobe in *Drosophila*. *Dev Biol* **404:** 61–75.

Akiyama-Oda Y, Hosoya T, Hotta Y. 1999. Asymmetric cell division of thoracic neuroblast 6-4 to bifurcate glial and neuronal lineage in *Drosophila*. *Development* **126:** 1967–1974.

Allen NJ, Barres BA. 2009. Glia - more than just brain glue. *Nature* **457:** 675–677.

Avet-Rochex A, Kaul AK, Gatt AP, McNeill H, Bateman JM. 2012. Concerted control of gliogenesis by InR/TOR and FGF signalling in the *Drosophila* post-embryonic brain. *Development* **139:** 2763–2772.

Awasaki T, Lai SL, Ito K, Lee T. 2008. Organization and postembryonic development of glial cells in the adult central brain of *Drosophila*. *J Neurosci* **28:** 13742–13753.

Baalman K, Marin MA, Ho TSY, Godoy M, Cherian L, Robertson C, Rasband MN. 2015. Axon initial segment-associated microglia. *J Neurosci* **35:** 2283–2292.

Babcock M. 2004. Genetic analysis of soluble N-ethylmaleimide-sensitive factor attachment protein function in *Drosophila* reveals positive and negative secretory roles. *J Neurosci* **24:** 3964–3973.

Ballard SL, Miller DL, Ganetzky B. 2014. Retrograde neurotrophin signaling through Tollo regulates synaptic growth in *Drosophila*. *J Cell Biol* **204:** 1157–1172.

Battefeld A, Klooster J, Kole MHP. 2016. Myelinating satellite oligodendrocytes are integrated in a glial syncytium constraining neuronal high-frequency activity. *Nat Commun* **7:** 1–13.

Bezzi P, Gundersen V, Galbete JL, Seifert G, Steinhäuser C, Pilati E, Volterra A. 2004. Astrocytes contain a vesicular compartment that is competent for regulated exocytosis of glutamate. *Nat Neurosci* **7:** 613–620.

Buchanan RL, Benzer S. 1993. Defective glia in the *Drosophila* brain degeneration mutant drop-dead. *Neuron* **10:** 839–850.

Bushong EA, Martone ME, Ellisman MH. 2004. Maturation of astrocyte morphology and the establishment of astrocyte domains during postnatal hippocampal development. *Int J Dev Neurosci* **22:** 73–86.

Christie K, Koshy D, Cheng C, Guo G, Martinez JA, Duraikannu A, Zochodne DW. 2015. Intraganglionic interactions between satellite cells and adult sensory neurons. *Mol Cell Neurosci* **67:** 1–12.

Christopherson KS, Ullian EM, Stokes CCA, Mullowney CE, Hell JW, Agah A, Lawler J, Mosher DF, Bornstein P, Barres BA. 2005. Thrombospondins are astrocyte-secreted proteins that promote CNS synaptogenesis. *Cell* **120:** 421–433.

Chung W-S, Clarke LE, Wang GX, Stafford BK, Sher A, Chakraborty C, Joung J, Foo LC, Thompson A, Chen C, et al. 2013. Astrocytes mediate synapse elimination through MEGF10 and MERTK pathways. *Nature* **504:** 394–400.

Doherty J, Sheehan AE, Bradshaw R, Fox AN, Lu T-Y, Freeman MR. 2014. PI3K signaling and Stat92E converge to modulate glial responsiveness to axonal injury. *PLoS Biol* **12:** e1001985.

Dumstrei K, Wang F, Hartenstein V. 2003. Role of DE-cadherin in neuroblast proliferation, neural morphogenesis, and axon tract formation in. *J Neurosci* **23:** 3325–3335.

Dunst S, Kazimiers T, Zadow von F, Jambor H, Sagner A, Brankatschk B, Mahmoud A, Spannl S, Tomancak P, Eaton S, et al. 2015. Endogenously tagged Rab proteins: a resource to study membrane trafficking in *Drosophila*. *Dev Cell* **33:** 351–365.

Egervari K, Potter G, Guzman-Hernandez ML, Salmon P, Soto-Ribeiro M, Kastberger B, Balla T, Wehrle-Haller B, Kiss JZ. 2015. Astrocytes spatially restrict VEGF signaling by polarized secretion and incorporation of VEGF into the actively assembling extracellular matrix. *Glia* **64:** 440–456.

Freeman MR, Doe CQ. 2001. Asymmetric Prospero localization is required to generate mixed neuronal/glial lineages in the *Drosophila* CNS. *Development* **128:** 4103–4112.

Freeman MR, Delrow J, Kim J, Johnson E, Doe CQ. 2003. Unwrapping glial biology: Gcm target genes regulating glial development, diversification, and function. *Neuron* **38:** 567–580.

Hanson PI, Otto H, Barton N, Jahn R. 1995. The N-ethylmaleimide-sensitive fusion protein and α-SNAP induce a conformational change in syntaxin. *J Biol Chem* **270:** 16955–16961.

Harward SC, Hedrick NG, Hall CE, Parra-Bueno P, Milner TA, Pan E, Laviv T, Hempstead BL, Yasuda R, McNamara JO. 2016. Autocrine BDNF–TrkB signalling within a single dendritic spine. *Nature* **538:** 99–103.

Hedrick NG, Harward SC, Hall CE, Murakoshi H, McNamara JO, Yasuda R. 2016. Rho GTPase complementation underlies BDNF- dependent homo- and heterosynaptic plasticity. *Nature* **538:** 104–108.

Huang L-YM, Gu Y, Chen Y. 2013. Communication between neuronal somata and satellite glial cells in sensory ganglia. *Glia* **61:** 1571–1581.

Ito K, Urban J, Technau GM. 1995. Distribution, classification, and development of *Drosophila* glial cells in the late embryonic and early larval ventral nerve cord. *Rouxs Arch Dev Biol* **204:** 284–307.

Jenett A, Rubin GM, Ngo T-TB, Shepherd D, Murphy C, Dionne H, Pfeiffer BD, Cavallaro A, Hall D, Jeter J, et al. 2012. A GAL4-driver line resource for *Drosophila* neurobiology. *Cell Rep* **2:** 991–1001.

Kim H-J, Cho M-H, Shim WH, Kim JK, Jeon E-Y, Kim D-H, Yoon S-Y. 2017. Deficient autophagy in microglia impairs synaptic pruning and causes social behavioral defects. *Mol Psychiatry* **22:** 1576–1584.

Kremer MC, Jung C, Batelli S, Rubin GM, Gaul U. 2017. The glia of the adult *Drosophila* nervous system. *Glia* **65:** 606–638.

Kurant E, Axelrod S, Leaman D, Gaul U. 2008. Six-microns-under acts upstream of Draper in the glial phagocytosis of apoptotic neurons. *Cell* **133:** 498–509.

Lazo OM, Gonzalez A, Ascano M, Kuruvilla R, Couve A, Bronfman FC. 2013. BDNF regulates Rab11-mediated recycling endosome dynamics to induce dendritic branching. *J Neurosci* **33:** 6112–6122.

Lee T, Luo L. 1999. Mosaic analysis with a repressible neurotechnique cell marker for studies of gene function in neuronal morphogenesis. *Neuron* **22:** 451–461.

Littleton JT, Chapman ER, Kreber R, Garment MB, Carlson SD, Ganetzky B. 1998. Temperature-sensitive paralytic mutations demonstrate that synaptic exocytosis requires SNARE complex assembly and disassembly. *Neuron* **21:** 401–413.

Luan H, Peabody NC, Vinson CR, White BH. 2006. Refined spatial manipulation of neuronal function by combinatorial restriction of transgene expression. *Neuron* **52:** 425–436.

Ma Z, Stork T, Bergles DE, Freeman MR. 2016. Neuromodulators signal through astrocytes to alter neural circuit activity and behaviour. *Nature* **539:** 428–432.

MacDonald JM, Beach MG, Porpiglia E, Sheehan AE, Watts RJ, Freeman MR. 2006. The *Drosophila* cell corpse engulfment receptor Draper mediates glial clearance of severed axons. *Neuron* **50:** 869–881.

McIlroy G, Foldi I, Aurikko J, Wentzell JS, Lim MA, Fenton JC, Gay NJ, Hidalgo A. 2013. Toll-6 and Toll-7 function as neurotrophin receptors in the *Drosophila melanogaster* CNS. *Nat Neurosci* **16:** 1248–1256.

Melom JE, Littleton JT. 2013. Mutation of a NCKX eliminates glial microdomain calcium oscillations and enhances seizure susceptibility. *J Neurosci* **33:** 1169–1178.

Muthukumar AK, Stork T, Freeman MR. 2014. Activity-dependent regulation of astrocyte GAT levels during synaptogenesis. *Nat Neurosci* **17:** 1340–1350.

Nimmerjahn A, Kirchhoff F, Helmchen F. 2005. Resting microglial cells are highly dynamic surveillants of brain parenchyma in vivo. *Science* **308:** 1314–1318.

Orr-Weaver TL. 2015. When bigger is better: the role of polyploidy in organogenesis. *Trends Genet* **31:** 307–315.

Parker JS, Mizuguchi K, Gay NJ. 2001. A family of proteins related to Spätzle, the toll receptor ligand, are encoded in the *Drosophila* genome. *Proteins* **45:** 71–80.

Paukert M, Agarwal A, Cha J, Doze VA, Kang JU, Bergles DE. 2014. Norepinephrine controls astroglial responsiveness to local circuit activity. *Neuron* **82:** 1263–1270.

Pereanu W, Shy D, Hartenstein V. 2005. Morphogenesis and proliferation of the larval brain glia in *Drosophila*. *Dev Biol* **283:** 191–203.

Pfeiffer BD, Jenett A, Hammonds AS, Ngo T-TB, Misra S, Murphy C, Scully A, Carlson JW, Wan KH, Laverty TR, et al. 2008. Tools for neuroanatomy and neurogenetics in *Drosophila*. *Proc Natl Acad Sci* **105:** 9715–9720.

Rabouille C, Kondo H, Newman R, Hui N, Freemont P, Warren G. 1998. Syntaxin 5 is a common component of the NSF- and p97-mediated reassembly pathways of Golgi cisternae from mitotic Golgi fragments in vitro. *Cell* **92:** 603–610.

Sherman DL, Brophy PJ. 2005. Mechanisms of axon ensheathment and myelin growth. *Nat Rev Neurosci* **6:** 683–690.

Smith CJ, Johnson K, Welsh TG, Barresi MJF, Kucenas S. 2016. Radial glia inhibit peripheral glial infiltration into the spinal cord at motor exit point transition zones. *Glia* **64:** 1138–1153.

Sorvina A, Shandala T, Brooks DA. 2016. *Drosophila* Pkaap regulates Rab4/Rab11-dependent traffic and Rab11 exocytosis of innate immune cargo. *Biol Open* **5:** 678–688.

Stork T, Sheehan A, Tasdemir-Yilmaz OE, Freeman MR. 2014. Neuron-glia interactions through the heartless FGF receptor signaling pathway mediate morphogenesis of *Drosophila* astrocytes. *Neuron* **83:** 388–403.

Sutcliffe B, Forero MG, Zhu B, Robinson IM, Hidalgo A. 2013. Neuron-type specific functions of DNT1, DNT2 and Spz at the *Drosophila* neuromuscular junction. *PLoS One* **8:** e75902.

Takasaki C, Yamasaki M, Uchigashima M, Konno K, Yanagawa Y, Watanabe M. 2010. Cytochemical and cytological properties of perineuronal oligodendrocytes in the mouse cortex. *Eur J Neurosci* **32:** 1326–1336.

Tasdemir-Yilmaz OE, Freeman MR. 2014. Astrocytes engage unique molecular programs to engulf pruned neuronal debris from distinct subsets of neurons. *Genes Dev* **28:** 20–33.

Unhavaithaya Y, Orr-Weaver TL. 2012. Polyploidization of glia in neural development links tissue growth to blood-brain barrier integrity. *Genes Dev* **26:** 31–36.

Vissers JHA, Manning SA, Kulkarni A, Harvey KF. 2016. A *Drosophila* RNAi library modulates Hippo pathway-dependent tissue growth. *Nat Commun* **7:** 10368.

Volkenhoff A, Weiler A, Letzel M, Stehling M, Klämbt C, Schirmeier S. 2015. Glial glycolysis is essential for neuronal survival in *Drosophila*. *Cell Metabolism* **22:** 437–447.

Wu H-H, Bellmunt E, Scheib JL, Venegas V, Burkert C, Reichardt LF, Zhou Z, Fariñas I, Carter BD. 2009. Glial precursors clear sensory neuron corpses during development via Jedi-1, an engulfment receptor. *Nat Neurosci* **12:** 1534–1541.

Xu T, Ashery U, Burgoyne RD, Neher E. 1999. Early requirement for α-SNAP and NSF in the secretory cascade in chromaffin cells. *EMBO J* **18:** 3293–3304.

Zhu B, Pennack JA, McQuilton P, Forero MG, Mizuguchi K, Sutcliffe B, Gu C-J, Fenton JC, Hidalgo A. 2008. *Drosophila* neurotrophins reveal a common mechanism for nervous system formation. *PLoS Biol* **6:** e284.